Available online at www.sciencedirect.com
ScienceDirect
Solid-State Electronics 51 (2007) 299–305
SOLID-STATE ELECTRONICS
www.elsevier.com/locate/sse

Volume inversion mobility in SOI MOSFETs for different thin body orientations

V. Sverdlov *, E. Ungersboeck, H. Kosina, S. Selberherr

Institute for Microelectronics, TU Vienna, Gusshausstr. 27–29, A-1040 Vienna, Austria

The review of this paper was arranged by Raphaël Clerc, Olivier Faynot and Nelly Kernevez

Abstract

Low field mobility in double- and single-gate structures is analyzed for (1 0 0) and (1 1 0) SOI substrate orientation. A Monte Carlo algorithm for vanishing driving fields allows the calculation of the mobility for arbitrary scattering rates and band structure without further approximations. Due to volume inversion, mobility in double-gate ultra-thin body (1 1 0) SOI FETs is enhanced in comparison with the mobility of single-gate structures in the whole effective field range. In double-gate (1 0 0) structures the mobility decreases below the single-gate value for high effective fields. It is argued that the twice as high carrier concentration in double-gate FETs causes significant occupation of higher subbands, where mobility is low, and that additional inter-subband scattering channels for the lowest subband are opened. These effects partly compensate the mobility enhancement due to volume inversion and lead to a mobility decrease in double-gate (1 0 0) structures.
© 2007 Elsevier Ltd. All rights reserved.

Keywords: Double-gate MOSFETs; Volume inversion; Mobility; Monte Carlo simulations

1. Introduction

Due to aggressive downscaling of transistor feature-size the role of parasitic short-channel effects in bulk MOSFETs is rapidly increasing, prompting for an introduction of alternative MOSFET architectures. Double-gate (DG) silicon-on-insulator (SOI) transistors with ultra-thin Si body (UTB) are considered to be good candidates for the far-end ITRS roadmap scaling [1]. Excellent electrostatic channel control in DG operation is theoretically predicted and allows scaling of the MOSFET's channel length down to 2.5 nm [2], maintaining reasonable subthreshold slope, satisfactory DIBL, and acceptable gain.

Despite the extensive experimental data available on mobility behavior in UTB FETs in DG and single-gate (SG) operation mode as well as the vast number of simulations for either SG or DG structures, a comparative theoretical analysis of mobility behavior in SG and DG FETs is limited to a few publications dealing exclusively with (1 0 0) SOI orientation [3,4]. Such an analysis is desirable due to an existing discrepancy between the mobility measurements and theoretical predictions for (1 0 0) UTB SOI FETs. At high effective fields the mobility measured in DG structures is smaller than the SG mobility [5], although an enhancement due to bulk inversion would be anticipated [6].

According to the volume inversion concept, in DG structures the inversion layers initially located at the opposite SOI interfaces intersect, leading to a charge maximum in the middle of the UTB. The charge is further away from the two rough interfaces, which eventually results in a mobility increase. Mobility behavior consistent with the bulk inversion concept was recently confirmed experimentally [7] in (1 1 0) UTB FETs: the DG mobility was higher than the SG mobility in the whole range of concentrations. In order to explain the observed behavior one has to theoretically compare the mobility behavior in SG and DG

* Corresponding author.
E-mail address: sverdlov@iue.tuwien.ac.at (V. Sverdlov).

0038-1101/$ - see front matter © 2007 Elsevier Ltd. All rights reserved.
doi:10.1016/j.sse.2007.01.022

structures for different body orientations. Contrary to the bulk MOSFET, the UTB FET must be intrinsic in order to avoid strong fluctuations of device characteristics due to the sensitivity to the random dopant positions. Absence of impurity scattering increases the mobility. At the same time important scattering mechanisms limiting the carrier mobility, such as electron–phonon interaction [8–10], surface roughness scattering [11,12], Si body thickness fluctuations [5], scattering with interface charges, and remote Coulomb scattering with impurities in the poly-gate [13,14] have been a subject of recent theoretical and experimental studies. It was recently re-confirmed that inter-subband scattering plays an important role in inversion layer mobility degradation [14,15]. Inter-subband scattering becomes especially pronounced in UTB FETs at high effective fields, when degeneracy effects due to Fermi statistics become important. Although the Fermi blocking factor cancels out from the scattering integral for elastic processes, it cannot be ignored for inelastic scattering even when it is small. Should the Pauli exclusion principle be omitted in the inelastic part of the scattering integral, the equilibrium distribution would simply be the Boltzmann distribution. With the blocking factor included inelastic scattering guarantees the Fermi–Dirac distribution at equilibrium. Fermi–Dirac statistics affects the mobility in UTB FETs because of two reasons: (i) higher subbands with lower mobilities are significantly populated, and (ii) additional inter-subband scattering channels within the ground subband are activated, if higher subbands are occupied. Accurate inclusion of the degeneracy effects due to the Pauli exclusion principle into the simulation schemes is essential for correct treatment of scattering and it is crucial for mobility calculations.

In this work we carry out a study of the mobility in SG and DG UTB FETs for different substrate orientations. A Monte Carlo algorithm is used which incorporates degeneracy effects *exactly* in the limit of vanishing driving fields and is valid for arbitrary scattering mechanisms and for general band structure [16]. We demonstrate that the doubled carrier concentration in DG structures leads to higher occupation of subbands with low mobilities and increases inter-subband scattering in (100) UTB FETs. These effects compensate the mobility enhancement due to volume inversion.

2. Simulation method

Degeneracy effects have an important influence on the mobility at high effective fields. The phonon-limited mobility calculated by a two-dimensional subband Monte Carlo method is quite different in degenerate and non-degenerate cases [17]. Surprisingly, if also surface scattering is included, the universal mobility curve can be reproduced using both degenerate and non-degenerate statistics [17]. However, in UTB FETs degeneracy effects are more pronounced, and their proper incorporation is crucial for accurate transport calculations.

Different approaches are known to include degeneracy into Monte Carlo algorithms. One method is to compute the occupation numbers self-consistently [18,19]. This approach is applicable not only to mobility simulations at equilibrium but also for higher driving fields [20]. When the distribution function is close to the equilibrium solution, the blocking factor can be approximated with the Fermi–Dirac distribution function [21]. The Kubo-Greenwood method is an attractive alternative to compute linear response functions. It leads to a set of integral equations for the relaxation times and requires simplifying approximations, which can be justified for isotropic bands in case of either elastic or isotropic inelastic scattering [11,14]. It is therefore desirable to have a tool which is formally exact in the limit of vanishing driving fields.

We generalize the Monte Carlo algorithm designed for small signal analysis of the three-dimensional electron gas [16] to quasi-two dimensional electron systems. The method is based on the solution of the linearized Boltzmann equation and is formally exact at small driving fields, and valid for arbitrary scattering mechanisms and band structure, including multi-valley and multi-subband case. The mobility tensor $\mu_{\alpha\beta}$ is calculated as follows:

(i) Initialize $t=0$, $w_\beta=0$, $v_{\alpha\beta}=0$, $\mu_{\alpha\beta}=0$, and start the particle trajectory with the stochastic dynamics determined by the scattering rates $\Lambda_{mn}(\mathbf{k},\mathbf{k}')$ of the *linearized* multi-subband Boltzmann equations. They are related to the rates $S_{mn}(\mathbf{k},\mathbf{k}')$ of the original Boltzmann equation via

$$\Lambda_{mn}(\mathbf{k}',\mathbf{k}) = (1-f(E_m(\mathbf{k}')))S_{mn}(\mathbf{k}',\mathbf{k}) + f(E_m(\mathbf{k}'))S_{mn}(\mathbf{k},\mathbf{k}'),$$

where $E_n(\mathbf{k})$ is the total electron energy in the nth two-dimensional subband.

(ii) Before each scattering event update $v_{\alpha\beta}$, w_β, and t

$$t = t + \frac{\tau(j)}{1-f(E(j))},$$
$$w_\beta = w_\beta + v_\beta(j)\tau(j),$$
$$v_{\alpha\beta} = v_{\alpha\beta} + \tau(j)v_\alpha(j)w_\beta(j),$$
$$\mu_{\alpha\beta} = \frac{e}{k_B T}\frac{v_{\alpha\beta}}{t},$$

where $v_\alpha(j)$ denotes the α-component of the velocity, $E(j)$ is the particle energy, $f(E)$ is the Fermi–Dirac function, and $\tau(j)$ is the time of jth free flight. The convergence of the method is improved by resetting $w_\beta=0$ if a velocity randomizing scattering event occurs.

The multi-subband generalization of the method requires the subband energies and wave functions to be pre-calculated self-consistently, for each value of the effective field. The transport calculations account for electron–phonon interaction [8,9] and surface roughness scattering, which are the dominant mechanisms determining the

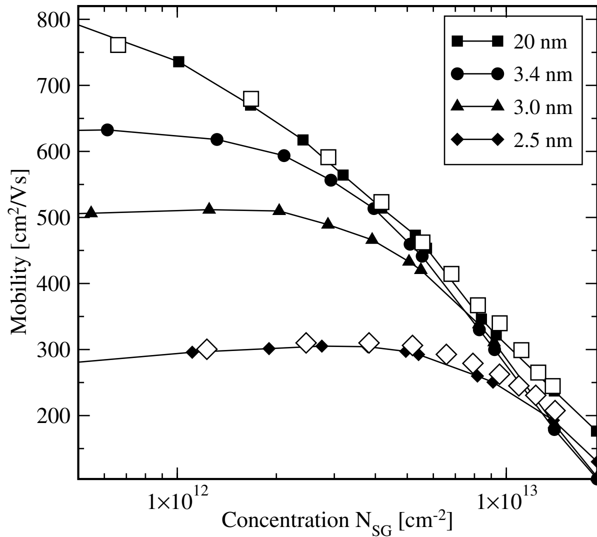

Fig. 1. Mobility simulations for SG (100) SOI FETs (filled symbols). Results are in good agreement with those reported previously [12] (open symbols).

mobility in the region of high effective fields. This captures the main difference of the mobility behavior in DG and SG structures at high concentrations for different orientations, as we demonstrate below.

In order to validate the computation procedure, we compare the results of mobility simulations with data available in the literature [12], see Fig. 1. Our simulations are in good agreement with previous calculations for 20 nm and 2.5 nm thick (100) UTB FETs, assuming similar surface roughness scattering parameters.

Mobility in a SG (100) UTB FET is compared for degenerate and non-degenerate statistics. Fig. 2 shows that neglecting the Fermi blocking factor leads to a significant overestimation of mobility, especially at higher carrier concentrations. The difference between the mobility values for degenerate and non-degenerate statistics looks surprising. Indeed, at high carrier concentrations the principal scattering mechanism limiting the low-field mobility is elastic surface roughness scattering. For elastic scattering the forward and inverse scattering rates are equal, and the Pauli blocking factor cancels out from the equations for the elastic scattering rates. However, the Pauli blocking factor is also present in the inelastic electron–phonon part of the total scattering integral and ensures the equilibrium solution to be the Fermi–Dirac distribution function. In the degenerate case the higher value of the Fermi level may open additional channels for inter-subband scattering, which reduces the mobility.

3. Simulation results for SG and DG mobilities

After the surface roughness parameters were calibrated to reproduce the bulk (100) surface mobility, we use the same model parameters to simulate mobilities of SG and DG (100) structures. Results are compared in Fig. 3 for several Si body thicknesses. For a 20 nm thick Si body the two inversion layers formed at the opposite interfaces of the DG structure are well separated and independent. The DG FET mobility plotted as a function of the concentration per single channel is in good agreement with the results for a SG structure. Both curves are in reasonable agreement with experimental data for a 32 nm thick Si

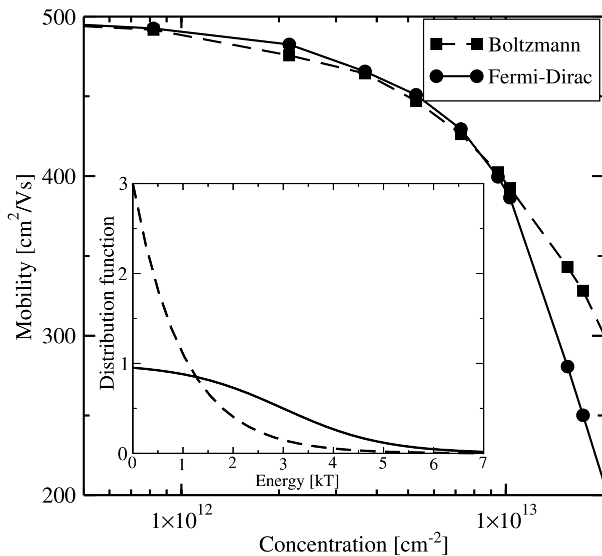

Fig. 2. Mobility simulations for a 3 nm thick SG structure, using Boltzmann and Fermi–Dirac statistics. Mobility calculated without Pauli exclusion principle taken into account is overestimated at high carrier concentrations. It is due to different subband population for the same N_s, with and without degeneracy effects included. Inset: Boltzmann and Fermi–Dirac distributions for the same temperature and N_s.

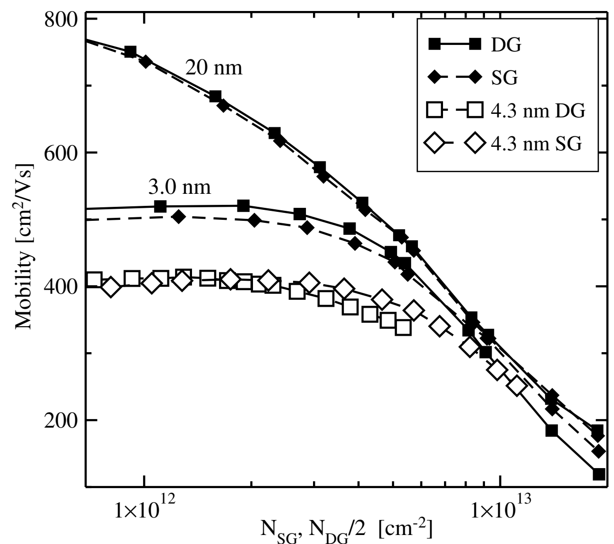

Fig. 3. Mobility for (100) UTB FETs. Mobility is plotted as a function of concentration for the SG structure and as a function of half of the concentration for the DG structure. Mobility in the DG structure is smaller than that in the SG structure at high concentration, which is in qualitative agreement with the experimental data [5] and in contrast to the bulk inversion concept [6].

body [7] and reproduce the universal mobility curve [22]. For 3 nm body thickness the DG mobility, plotted as a function of $N_s/2$, tends to be slightly higher at small effective fields. For high N_s the DG mobility for (1 0 0) orientation becomes lower than the SG mobility. This is in qualitative agreement with experimental data, also shown in Fig. 3. This behavior, however, contradicts the volume inversion concept [6]. According to this concept in volume inversion carriers are located in the center of the Si body and are further away from the interfaces. Due to reduced surface roughness scattering the mobility in a DG structure is expected to be higher than the mobility in a SG structure.

It should be noted that in order to obtain a better quantitative agreement with the experimental mobility, additional mechanisms such as surface optical phonons interaction, or scattering on fluctuations of δT_{SOI} [23] could be included. Introduction of acoustic phonon confinement relevant to UTB FET structures also improves agreement with the experimental data [24]. However, our model captures the main difference in the mobility behavior in DG and SG structures at high concentrations, namely that the DG mobility is lower than the SG mobility. It should also be noted that in DG structures the mobility plotted as a function of the total concentration is always higher than in SG structures, as was pointed out in [25].

Using a thick body DG FET, we demonstrate the importance of inter-subband scattering for mobility calculations. For a thick DG structure the wave functions $\psi_i(z)$ corresponding to two independent inversion layers $i = 1, 2$ are located at the opposite interfaces. Due to the large separation between the interfaces, the value of the wave function and its derivatives is zero at the interface opposite to its location. By making symmetric $\psi_+(z)$ and asymmetric $\psi_-(z)$ combinations of $\psi_1(z)$ and $\psi_2(z)$, one obtains the wave functions corresponding to the first and the second subband in the Si body

$$\psi_\pm(z) = \frac{1}{\sqrt{(2)}}(\psi_1(z) \pm \psi_2(z)). \tag{1}$$

For the sake of simplicity let us consider surface roughness scattering only at the left interface, $z = 0$. The surface roughness scattering rate $\Gamma_{ij}(q)$ between the two subbands k and j is proportional to [26]

$$\Gamma_{kj} = \left(\frac{\hbar^2}{2m_z}\right)^2 \left(\frac{d\psi_k(0)}{dz}\right)^2 \left(\frac{d\psi_j(0)}{dz}\right)^2, \tag{2}$$

where the derivative $d\psi_k(0)/dz$ of the kth wave function is computed at the interface $z = 0$, and m_z is the quantization mass. For a thick body FET it holds $d\psi_2(0)/dz = 0$, and the total scattering rate within the first subband $\psi_+(z)$ is

$$\Gamma_+ = \Gamma_{++} + \Gamma_{+-} = \frac{1}{2}\left(\frac{\hbar^2}{2m_z}\right)^2 \left(\frac{d\psi_1(0)}{dz}\right)^4, \tag{3}$$

where both Γ_{++} and Γ_{-+} are

$$\Gamma_{++} = \Gamma_{-+} = \frac{1}{4}\left(\frac{\hbar^2}{2m_z}\right)^2 \left(\frac{d\psi_1(0)}{dz}\right)^4. \tag{4}$$

Therefore, a half of the total scattering rate would be missed if the inter-subband scattering were neglected. A similar conclusion also holds for electron–phonon scattering [27].

Now we turn our attention to (1 1 0) UTB FETs. Due to the surface orientation, the effective equation for the envelope functions in quantization direction contains also the first order derivative of the wave functions. The derivative can be removed from the equation by a wave function transformation [28], which results in a standard Schrödinger-like equation for the envelope function in the quantization direction, allowing the determination of quantization mass, conductivity mass and density-of-state effective mass. For (1 1 0) orientation the subband structure consists of a 4-fold and a 2-fold degenerate subband ladder. Subbands in both ladders are anisotropic. Simulation results for 20 nm thick SG and DG structures are shown in Fig. 4. The results for SG and DG structures, which are plotted as a function of the concentration per inversion layer, are in good agreement with each other and with experimental data [7]. Due to the high anisotropy of the subbands of each ladder the surface mobility is anisotropic. Diagonal values of the mobility tensor along $\langle 0 0 1\rangle$ and $\langle 1 \bar{1} 0\rangle$ directions are in agreement with those observed experimentally [7].

Fig. 5 shows results of mobility simulations in $\langle 1 \bar{1} 0\rangle$ direction performed for several Si body thicknesses using the same scattering parameters as for thick Si films. The mobility of (1 1 0) UTB FETs coincides reasonably well with the experimental data [7] shown in Fig. 5. The mobility for (1 1 0) DG structures is higher than the mobility of

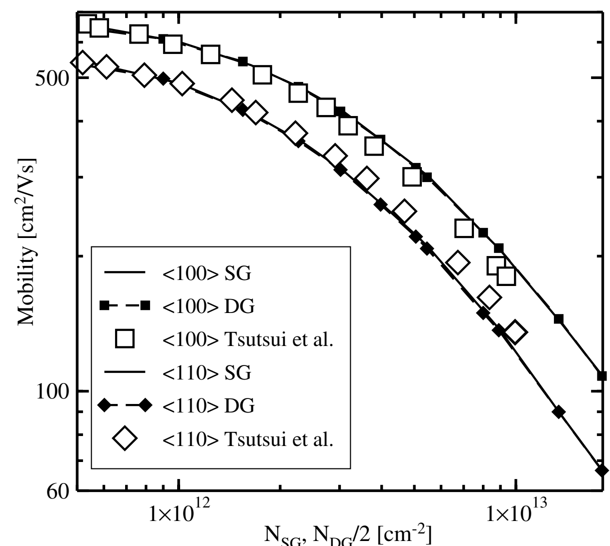

Fig. 4. Low field mobility in different directions calculated for 20 nm (1 1 0) SG and DG structures (filled symbols) closely follows experimental data [7] (open symbols). Mobility tensor components per inversion layer in thick DG and SG structures are the same.

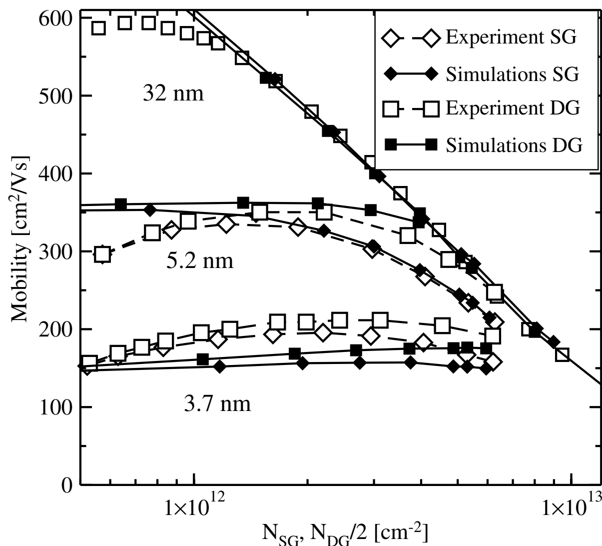

Fig. 5. Mobility in $\langle 1\bar{1}0\rangle$ direction for SG and DG structures with (1 1 0) thin body orientation. Mobility is plotted as a function of concentration for SG structures and as function of half the concentration for DG structures. DG (1 1 0) UTB mobility is higher than the SG mobility in whole range of concentrations, in good agreement with the experimental data [7], supporting the bulk inversion concept [6].

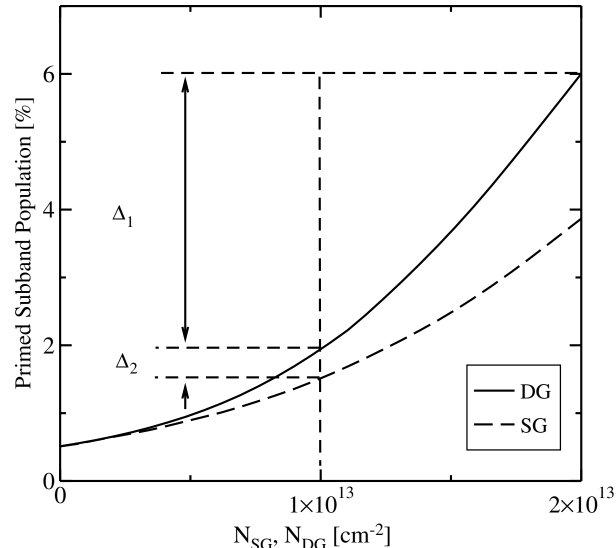

Fig. 6. Occupation of primed ladder in a 3 nm thick (1 0 0) UTB FET as a function of total concentration for either SG or DG operation mode. Higher primed ladder occupation in DG FET is mainly due to the Δ_2 contribution resulting from twice-as-high carrier concentration in DG as compared to SG FETs, for similar gate voltage. Contribution Δ_2 due to subband structure difference [7] is small.

(1 1 0) SG structures in the whole concentration range. It is consistent with recent experimental studies [7] and confirms the concept of the mobility enhancement in DG UTB FETs due to volume inversion [6].

4. Volume inversion in (1 1 0) and (1 0 0) UTB FETs

Mobility in a (1 0 0) UTB double-gate FET plotted as function of carrier concentration per inversion layer becomes lower than the mobility in a corresponding SG FET. This is in sharp contrast with results for (1 1 0) FETs mobilities and is in obvious contradiction with the concept of the mobility enhancement due to volume inversion. In order to explain the apparent contradiction, high occupation of primed subbands in (1 0 0) DG FETs with a significantly lower mobility caused by heavier conductivity mass was assumed in [7]. The higher occupation of primed subbands in DG FETs was justified by smaller energy splitting between the lowest primed and unprimed subbands in in a (1 0 0) DG FET induced by the interaction of the inversion layers [7]. However, in UTB FETs the subband structure is mainly determined by strong geometrical confinement. Therefore, the subband structure and the occupation of subbands should be quite similar in UTB DG and SG FETs provided the total carrier concentration is the same in both structures. At the same time the SG and DG mobilities should be compared for the same gate voltages. In case of an intrinsic body this corresponds to the mobilities compared as functions of the concentration per single inversion layer. Since in a DG FET there are two inversion layers created at the front and the back interface of the Si body, the total concentration in a DG structure is twice as high as in a SG structure for the same gate voltage. Also due to the double carrier concentration the occupation of the primed subbands can be higher in DG structures.

In order to compare relative contributions of two different mechanisms to increase of the primed subband occupation in a DG FET with a SG FET, in Fig. 6 we plot the occupation of the primed subband ladder as a function of the total concentration in SG and DG structures. The contribution Δ_2 computed at the same total concentration is due to the difference in energy splitting between primed and unprimed ladders and corresponds to the mechanism proposed in [7]. This contribution plays a minor role compared to the increase Δ_1 of the primed subband occupation due to the doubled carrier concentration in DG structures for similar gate voltages.

If we now apply similar argumentation to (1 1 0) UTB FETs, we arrive to similar conclusions. Namely, the occupation of primed subbands increases rapidly in DG (1 1 0) UTB FETs at high effective fields, which should also lead to a more rapid decrease of DG mobility in (1 1 0) FETs due to the lower mobility in primed subbands. However, this conclusion contradicts the experimental data and the results of simulations. Higher occupancy of primed subbands in DG structures is present in both (1 0 0) and (1 1 0) UTB FETs and cannot be the only reason for the mobility lowering observed in DG (1 0 0) structures.

Due to different quantization masses, the subband structures in (1 0 0) and (1 1 0) UTB FETs differ significantly. In (1 0 0) UTB FETs the subband energy of the second unprimed subband is nearly equal to the energy of the first primed subband, while in (1 1 0) FETs the second unprimed 4-fold degenerate subband lies significantly higher than the

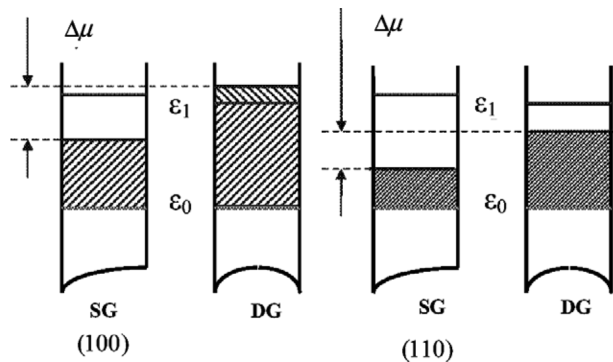

Fig. 7. Illustration of higher unprimed subband occupation in (1 0 0) and (1 1 0) UTB FETs. Contrary to (1 1 0) FETs, the higher unprimed subbands are occupied significantly in DG (1 0 0) FETs, for the same concentrations, due to a heavier quantization mass and a lighter in-plane density-of-states mass.

lowest primed subband. Even though the occupation of primed subbands increases for both (1 0 0) and (1 1 0) orientations with increasing effective field, higher unprimed subbands remain virtually de-populated in (1 1 0) UTB FETs. Contrary, the occupation of higher unprimed subbands increases rapidly in DG (1 0 0) FETs for high effective fields. Fig. 7 illustrates the higher unprimed subband occupation in (1 0 0) compared to (1 1 0) DG FETs.

Fig. 8 shows a strong correlation between the rapid mobility degradation and the occupation increase of the higher unprimed subbands in a (1 0 0) DG structure. However, estimations demonstrate that the fraction of carriers occupying the higher subbands is not sufficient to cause such a significant drop in the DG (1 0 0) FET mobility. A more substantial correction comes from the mobility lowering in the ground subband itself. Since the higher unprimed subband is occupied in (1 0 0) DG structures, an extra channel of scattering between the ground and the second

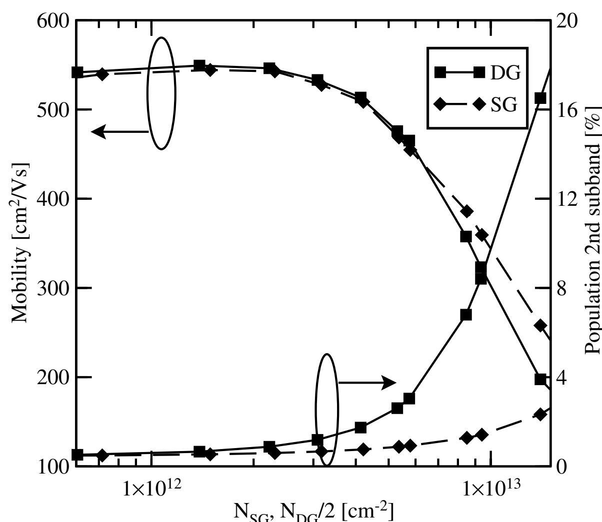

Fig. 8. Correlation between mobility degradation and occupation of higher unprimed subbands in a 3 nm thick DG (1 0 0) SOI FET.

unprimed subbands opens. This mechanism plays a significant role in the (1 0 0) DG mobility lowering: If we switch off the inter-subband scattering in the simulations, thus forbidding the scattering between the lowest and higher unprimed subbands, the DG mobility exceeds the corresponding (1 0 0) SG mobility, even at high carrier concentrations, in compliance with the volume inversion concept.

5. Conclusion

The mobility in DG and SG UTB FETs for different Si orientations was investigated theoretically. Our method is based on the solution of the linearized Boltzmann equation and allows the exact treatment of the Pauli exclusion principle in the limit of vanishing driving fields. This method is valid for arbitrary scattering rates and includes realistic band structures. Our results are in good agreement with experimental data for (1 1 0) UTB FETs, confirming the mobility enhancement in DG operation mode over the SG operation mode due to volume inversion. It is shown that two effects compensate the volume inversion induced mobility enhancement in (1 0 0) DG structures. These effects are a significant occupation of higher subbands in the unprimed ladder as well as an extra channel of intersubband scattering, which decreases the mobility in the lowest subband of DG (1 0 0) FETs. Due to different quantization masses, these effects are absent in (1 1 0) UTB FETs.

Acknowledgements

We gratefully acknowledge financial support from the Austrian Science Fund FWF, project P17285-N02, and the European Commission, project SINANO IST-506844.

References

[1] Likharev KK. Sub-20-nm electron devices. In: Morkoc H, editor. Advanced semiconductor and organic nano-techniques. New York: Academic Press; 2003. p. 239–302.
[2] Sverdlov V, Walls T, Likharev K. Nanoscale silicon MOSFETs: a theoretical study. IEEE Trans Electr Dev 2003;50(9):1926–33.
[3] Gámiz F, Roldán JB, Godoy A, Cartujo-Cassinello P, Carceller JE. Electron mobility in double gate silicon on insulator transistors: symmetric-gate versus asymmetric-gate configuration. J Appl Phys 2003;94(9):5732–41.
[4] Esseni D, Abramo A, Selmi L, Sangiorgi E. Physically based modeling of low field electron mobility in ultrathin single- and double-gate SOI n-MOSFETs. IEEE Trans Elect Dev 2003;50(12):2445–55.
[5] Uchida K, Koga J, Takagi S. Experimental study on carrier transport mechanisms in double- and single-gate ultrathin-body MOSFETs – Coulomb scattering, volume inversion, and δT_{SOI}-induced scattering. In: IEDM Techn Dig 2003. p. 805–8.
[6] Balestra F, Cristoloveanu S, Benachir M, Brini J, Elewa T. Double-gate silicon-on-insulator transistor with volume inversion: a new device with greatly enhanced performance. IEEE Electr Dev Lett 1987;8(9):410–2.
[7] Tsutsui G, Saitoh M, Saraya T, Nagumo T, Hiramoto T. Mobility enhancement due to volume inversion in (1 1 0)-oriented ultra-thin body double-gate nMOSFETs with body thickness less than 5 nm. In: IEDM Techn Dig 2005. p. 747–50.

[8] Price PJ. Resonant tunneling via an accumulation layer. Ann Phys 1981;133:217.
[9] Jacoboni C, Reggiani L. The Monte Carlo method for the solution of charge transport in semiconductors with applications to covalent materials. Rev Mod Phys 1983;55(3):645–705.
[10] Lunstrom M. Fundamentals of carrier transport. Cambridge: Cambridge University Press; 2000.
[11] Fischetti MV, Ren Z, Solomon PM, Yang M, Rim K. Six-band K.P calculation of the hole mobility in silicon inversion layers: dependence on surface orientation, strain, and silicon thickness. J Appl Phys 2003;94(2):1079–95.
[12] Esseni D. On the modeling of surface roughness limited mobility in SOI MOSFETs and its correlation to the transistor effective field. IEEE Trans Electr Dev 2004;51(3):394–401.
[13] Gámiz F, Roldán JB, Carceller JE, Cartujo P. Monte Carlo simulation of remote-Coulomb-scattering-limited mobility in metal–oxide–semiconductor transistors. Appl Phys Lett 2003;82(19):3251–3.
[14] Esseni D, Abramo A. Modeling of electron mobility degradation by remote Coulomb scattering in ultrathin oxide MOSFETs. IEEE Trans Electr Dev 2003;50(7):1665–75.
[15] Lucci L, Esseni D, Palestri P, Selmi L. Conparative analysis of basic transport properties in the inversion layer of bulk and SOI MOSFETs: a Monte–Carlo study. In: Proc. Intl. Conf. on simulation of semiconductor processes and devices. München; 2004. p. 321–4.
[16] Smirnov S, Kosina H, Nedjalkov M, Selberherr S. Monte Carlo method for modeling of small signal response including the Pauli exclusion principle. J Appl Phys 2003;94(9):5791–9.
[17] Ungersboeck E, Kosina H. The effect of degeneracy on electron transport in strained silicon inversion layer. In: Proc. Intl. Conf. on simulation of semiconductor processes and devices. 2005. p. 311–4.
[18] Bosi S, Jacoboni C. Monte Carlo high field transport in degenerate GaAs. J Phys C Solid State Phys 1976;9:315–9.
[19] Lugli P, Ferry DK. Degeneracy in the ensemble Monte Carlo method for high field transport in semiconductors. IEEE Trans Electr Dev 1985;32(11):2431–7.
[20] Lucci L, Palestri P, Esseni D, Selmi L. Multi-subband Monte–Carlo modeling of nano-MOSFETs with strong vertical quantization and electron gas degeneration. In: IEDM Techn. Dig. 2005. p. 531–634.
[21] Fischetti M, Laux S. Monte Carlo analysis of electron transport in small semiconductor devices including band-structure and space-charge effects. Phys Rev B 1988;38(14):9721–45.
[22] Takagi SI, Toriumi A, Iwase M, Tango H. On the universality of inversion layer mobility in Si MOSFET's: Part I – effects of substrate impurity concentration. IEEE Trans Electr Dev 1994;41(12):2357–62.
[23] Esseni D, Abramo A. Mobility modelling of SOI MOSFETs. Semicond Sci Technol 2004;19:S67–70.
[24] Donetti L, Gámiz F, Rodriguez N, Jamenez F, Sampedro C. Influence of acoustic phonon confinement on electron mobility in ultrathin silicon on insulator layers. Appl Phys Lett 2006;88(1): 122108(1–3).
[25] Esseni D, Mastrapasqua M, Celler G, Fiegna C, Selmi L, Sangiorgi E. An experimental study of mobility enhancement mobility in ultrathin single- and double-gate SOI in ultrathin SOI transistors operated in double-gate mode. IEEE Trans Electr Dev 2003;50(3): 802–8.
[26] Prange RE, Nee TW. Quantum spectroscopy of the low-field oscillations in the surface impedance. Phys Rev 1968;168(3): 779–86.
[27] Shoji M, Horiguchi S. Electronic structure and phonon-limited electron mobility of double-gate silicon-on-incubator Si inversion layers. J Appl Phys 1999;85(5):2722–31.
[28] Stern F, Howard WE. Propersties of semiconductor surface inversion layers in the electric quantum limit. Phys Rev 1967;163(3):816–35.